

# Gridless sparse covariance-based beamforming via alternating projections including co-prime arrays

Yongsung Park<sup>a)</sup>  and Peter Gerstoft 

Scripps Institution of Oceanography, University of California San Diego, La Jolla, California 92093-0238, USA

## ABSTRACT:

This paper presents gridless sparse processing for direction-of-arrival (DOA) estimation. The method solves a gridless version of sparse covariance-based estimation using alternating projections. Gridless sparse DOA estimation is represented by the reconstruction of Toeplitz-structured low-rank matrices, which our method recovers by alternatively projecting a solution matrix. Compared to the existing gridless sparse methods, our method improves speed and accuracy and considers non-uniformly configured linear arrays. High-resolution and reliable DOA estimation are achieved even with single-snapshot data, coherent sources, and non-uniform arrays. Simulation results demonstrate performance improvements compared to the existing DOA estimators, including gridless sparse methods. The method is illustrated using experimental data from a real ocean experiment. © 2022 Acoustical Society of America.

<https://doi.org/10.1121/10.0011617>

(Received 11 November 2021; revised 23 April 2022; accepted 19 May 2022; published online 8 June 2022)

[Editor: James F. Lynch]

Pages: 3828–3837

## I. INTRODUCTION

Direction-of-arrival (DOA) estimation, beamforming, is finding the angle of each source arriving on an array of sensors. DOA estimation with a sparse representation motivates obtaining sharp estimates of the beamforming spectrum that achieve higher resolution over traditional estimators.<sup>1–3</sup> DOAs are continuous-valued in an angular domain, and gridless sparse processing estimates DOAs without a grid.<sup>4–6</sup> We propose a DOA estimation method for gridless sparse signal recovery.

Sparse signal representation or compressive sensing (CS)<sup>7</sup> promotes sparse solutions with sharp peaks in the beamforming spectrum, which exhibits high resolution. CS for DOA performs well with single-snapshot data and with coherent sources.<sup>1,3,8,9</sup> A grid of potential DOAs deteriorates DOA performance when true DOAs are not on the grid, called basis mismatch.<sup>10–12</sup>

Gridless CS<sup>13–15</sup> operates in a continuous angular domain and mitigates the basis mismatch.<sup>4–6,16–19</sup> Several gridless sparse processing methods have been introduced<sup>14</sup> and applied for DOA.<sup>6</sup> Some use snapshot data, e.g., atomic norm minimization (ANM),<sup>11,14,20</sup> while others use sample covariance matrix (SCM), e.g., gridless sparse iterative covariance-based estimation.<sup>6,8,21</sup> SCM methods use the data matrix with the number of sensors and reduce computational cost when many snapshot data are available. Connections among ANM-based methods and gridless sparse SCM methods are investigated in Refs. 6 and 20.

The gridless sparse methods have challenges, including accelerating solvers and arbitrary array geometries.<sup>6,14</sup> Standard convex solvers have been used to deal with semi-

definite programming, formulated for gridless sparse processing, and the solver is infeasible in practice for high-dimensional problems. The gridless sparse methods have a formulation limited to uniform linear arrays (ULAs) or sub-sampled ULAs, which are not applicable for arbitrary non-uniform structures. The methods for arbitrary array geometry have been presented,<sup>15–17,22</sup> and they use the Fourier series to approximate the non-uniform sampling into uniform sampling.<sup>13,23</sup>

Covariance fitting-based sparse processing methods are achieved by recovering a structured matrix close to the SCM.<sup>8,21,24,25</sup> The matrix has the lowest rank positive semi-definite (PSD) Toeplitz structure.<sup>24,26,27</sup> Any rank-deficient (less sources than sensors), PSD Toeplitz matrix is uniquely decomposed (the Vandermonde decomposition).<sup>6,20</sup> Using the decomposition, the DOAs are retrieved from the reconstructed matrix.

Structured matrix reconstruction is achieved by alternating projections (AP).<sup>28,29</sup> AP is an algorithm for finding a point in the intersection of some sets, using a series of projections onto the sets. AP has solved matrix completion,<sup>30–32</sup> phase retrieval,<sup>33–35</sup> and structured low-rank matrix reconstruction.<sup>36–38</sup> Gridless sparse DOA estimation is achieved by AP-based on the lowest rank PSD Toeplitz matrix recovery, called AP-Snapshot.<sup>39,40</sup>

We propose an AP method for gridless sparse DOA estimation, which uses covariance fitting, called AP-Covariance. AP-Covariance has the objective to recover a DOA-dependent SCM, which is a low rank Toeplitz matrix, and has the constraint with a PSD matrix. It consists of a sequence of two projections: low-rank Toeplitz projection and PSD projection.

AP methods for gridless sparse DOA estimation have the low-rank Toeplitz projection. We utilize the projection

<sup>a)</sup>Electronic mail: yongsungpark@ucsd.edu

scheme in AP-Snapshot<sup>39,40</sup> and replace the projection in the earlier AP-Covariance.<sup>41</sup> This significantly improves DOA accuracy for AP-Covariance. Further, the proposed low-rank Toeplitz projection deals with arbitrary non-uniform linear arrays (NUAs). The earlier AP-Covariance considers non-uniform arrays in the case of sub-sampled ULAs, not arbitrary configurations. The projection fits well with covariance fitting formulation and enables AP-Covariance to outperform AP-Snapshot. For NUA performance, we show DOA performance for co-prime arrays,<sup>42</sup> a popular NUA.

## II. ARRAY DATA MODEL

Consider  $K$  narrowband sources for  $L$  snapshot data with complex signal  $s_{k,l} \in \mathbb{C}$ ,  $k = 1, \dots, K$ ,  $l = 1, \dots, L$ . We assume the sources with DOAs  $\theta_k \in [-90^\circ, 90^\circ]$  are in the far-field of a linear array with  $M$  sensors and  $L$  snapshots. The observed array data  $\mathbf{Y} \in \mathbb{C}^{M \times L}$  and the SCM  $\tilde{\mathbf{R}} \in \mathbb{C}^{M \times M}$  are modeled as

$$\mathbf{Y} = \sum_{k=1}^K \mathbf{a}(\theta_k) \mathbf{s}_k^\top + \mathbf{E} = \sum_{k=1}^K c_k \mathbf{a}(\theta_k) \phi_k^\top + \mathbf{E}, \quad (1)$$

$$\tilde{\mathbf{R}} = \mathbf{Y} \mathbf{Y}^\text{H} / L, \quad (2)$$

where  $\mathbf{s}_k = [s_{k,1} \cdots s_{k,L}]^\top \in \mathbb{C}^L$ ,  $c_k = \|\mathbf{s}_k\|_2 > 0$ ,  $\phi_k = c_k^{-1} \mathbf{s}_k \in \mathbb{C}^L$  with  $\|\phi_k\|_2 = 1$ ,  $\mathbf{E} \in \mathbb{C}^{M \times L}$  is the additive noise, and the steering vector,

$$\mathbf{a}(\theta) = [e^{-j(2\pi/\lambda)d_1 \sin \theta} \cdots e^{-j(2\pi/\lambda)d_M \sin \theta}]^\top \in \mathbb{C}^M, \quad (3)$$

where  $\lambda$  is the wavelength. The distance between sensors 1 and  $m$  is  $d_m = \delta_m d$ ,  $m = 1, \dots, M$ , where  $\delta_m$  is a scale factor in units of sensor spacing  $d$  (here,  $d = \lambda/2$ ). A uniform linear array (ULA) has  $\boldsymbol{\delta} = [0 \ 1 \ \cdots \ M-1]^\top$ . NUAs consist of real number  $\delta_m$ .

## III. GRIDLESS SPARSE COVARIANCE DOA ESTIMATION AND ITS RANK MINIMIZATION REPRESENTATION

Assuming the sources  $\mathbf{s}_k$  and the noise  $\mathbf{E}$  are uncorrelated and  $\mathbb{E}\{\mathbf{s}_l\} = \text{diag}(\mathbf{p})$  and  $\mathbb{E}\{\mathbf{e}_l\} = \sigma^2 \mathbf{I}$ , the expected SCM [Eq. (2)] over snapshots is

$$\mathbb{E}\{\tilde{\mathbf{R}}\} = \sum_{k=1}^K c_k^2 \mathbf{a}(\theta_k) \mathbf{a}^\text{H}(\theta_k) + \sigma^2 \mathbf{I} = \text{Adiag}(\mathbf{p}) \mathbf{A}^\text{H} + \sigma^2 \mathbf{I}. \quad (4)$$

Without correlated terms, Eq. (2) converges to Eq. (4) as  $L \rightarrow \infty$ .<sup>43</sup> DOAs are estimated from under statistical assumptions,  $\tilde{\mathbf{R}} = \mathbb{E}\{\tilde{\mathbf{R}}\}$ .<sup>6,44–46</sup>

Gridless sparse iterative covariance-based estimation (GLS)<sup>6,20</sup> uses a parameter  $\mathbf{R} \in \mathbb{C}^{M \times M}$  and fits it to SCM  $\tilde{\mathbf{R}} (= \mathbb{E}\{\tilde{\mathbf{R}}\} = \text{Adiag}(\mathbf{p}) \mathbf{A}^\text{H} + \sigma^2 \mathbf{I})$ . The covariance fitting [handles both nonsingular and singular ( $L < M$ )  $\tilde{\mathbf{R}}$ ] is accomplished by minimizing (Refs. 6, p. 553 and 21)

$$\|\mathbf{R}^{-1/2}(\tilde{\mathbf{R}} - \mathbf{R})\|_\text{F}^2 = \text{tr}(\tilde{\mathbf{R}} \mathbf{R}^{-1} \tilde{\mathbf{R}}) + \text{tr}(\mathbf{R}) - 2\text{tr}(\tilde{\mathbf{R}}). \quad (5)$$

The resulting optimization is (Refs. 6, p. 553 and 21)

$$\min_{\mathbf{R}, \mathbf{Z}} \text{tr}(\mathbf{Z}) + \text{tr}(\mathbf{R}) \quad \text{subject to } \mathbf{P} = \begin{bmatrix} \mathbf{R} & \tilde{\mathbf{R}} \\ \tilde{\mathbf{R}} & \mathbf{Z} \end{bmatrix} \geq 0, \quad (6)$$

where  $\mathbf{P}$  is PSD,  $\mathbf{P} \geq 0$ , and  $\mathbf{Z} \in \mathbb{C}^{M \times M}$  is a free variable. When  $\mathbf{R}$  is noiseless, then  $\text{tr}(\mathbf{R}) = M \sum_{k=1}^K c_k^2$ . Defining  $\text{tr}(\mathbf{Z}) = M \sum_{k=1}^K c_k^2$ , the objective [Eq. (6)], divided by  $2M$ , is

$$\frac{1}{2M} \text{tr}(\mathbf{R}) + \frac{1}{2M} \text{tr}(\mathbf{Z}) = \sum_{k=1}^K c_k^2. \quad (7)$$

In the atomic norm minimization,<sup>11,14</sup> minimizing  $\sum_{k=1}^K c_k^2$  is equivalent to minimizing the atomic norm,

$$\|\mathbf{Y}^*\|_{\mathcal{A}} = \inf_{c_k, \theta_k, \phi_k} \left\{ \sum_{k=1}^K c_k : \mathbf{Y}^* = \sum_{k=1}^K c_k \mathbf{a}(\theta_k) \phi_k^\top \right\}. \quad (8)$$

This is a convex relaxation of the atomic  $l_0$  norm,<sup>11</sup>

$$\|\mathbf{Y}^*\|_{\mathcal{A},0} = \inf_{c_k, \theta_k, \phi_k} \left\{ K : \mathbf{Y}^* = \sum_{k=1}^K c_k \mathbf{a}(\theta_k) \phi_k^\top \right\}. \quad (9)$$

Minimizing Eq. (9) is equivalent to minimizing rank of  $\mathbf{R} = \mathbf{Y} \mathbf{Y}^\text{H} / L$ .<sup>6,11</sup> That is,  $\text{tr}(\mathbf{R}) = \sum_{k=1}^K c_k^2$  is the nuclear norm and is a convex relaxation of rank( $\mathbf{R}$ ).

GLS solves Eq. (6) to obtain  $\mathbf{R}$ , where  $\{\hat{\mathbf{A}}, \hat{\mathbf{p}}, \hat{\sigma}^2\}$  are estimates of  $\{\mathbf{A}, \mathbf{p}, \sigma^2\}$ . The noise variance  $\hat{\sigma}^2$  is estimated as the average of the smallest  $M - K$  eigenvalues of the resultant  $\mathbf{R}$  [Eq. (6)] (assuming the noise is the small eigenvalues).<sup>21,46</sup> Then, DOAs  $\hat{\theta}_k$  are estimated by factorizing  $\mathbf{R} - \hat{\sigma}^2 \mathbf{I} (= \hat{\mathbf{A}}(\hat{\theta}) \text{diag}(\hat{\mathbf{p}}) \hat{\mathbf{A}}(\hat{\theta})^\text{H})$ . The factorization is achieved via the Vandermonde decomposition, the same as in Eq. (12), which is computed via root-MUSIC (multiple signal classification)<sup>45</sup> in Eq. (14).<sup>11,14</sup>

Minimizing the nuclear norm  $\text{tr}(\mathbf{R} - \hat{\sigma}^2 \mathbf{I}) = \sum_{k=1}^K \hat{p}_k$  is a convex relaxation of rank( $\mathbf{R} - \hat{\sigma}^2 \mathbf{I}$ ).<sup>6,10</sup> The following rank minimization of Eq. (6) is

$$\min_{\mathbf{R}, \mathbf{Z}} \text{rank}(\mathbf{R} - \sigma^2 \mathbf{I}) \quad \text{subject to } \mathbf{P} = \begin{bmatrix} \mathbf{R} & \tilde{\mathbf{R}} \\ \tilde{\mathbf{R}} & \mathbf{Z} \end{bmatrix} \geq 0. \quad (10)$$

AP-Covariance solves Eq. (10), which is the same as in Ref. 41, but uses different projections in Sec. IV B. It minimizes  $\text{rank}(\mathbf{R} - \sigma^2 \mathbf{I})$  via the Vandermonde decomposition and estimates  $\sigma^2$  in the same manner as in GLS, but computed iteratively as  $\mathbf{R}$  is updated.

The formulation Eq. (10) is similar in AP-Snapshot,<sup>40</sup> except that  $\mathbf{P}$  consists of SCM  $\tilde{\mathbf{R}}$  rather than snapshot data  $\mathbf{Y}$ . Thus, AP-Covariance is covariance-based. Snapshot-data-fitting methods rely on complex source amplitudes  $\mathbf{S} = [\mathbf{s}_1 \cdots \mathbf{s}_K] \in \mathbb{C}^{L \times K}$  in data  $\mathbf{Y}$  [Eq. (1)]. Contrarily, covariance-fitting methods rely on the source covariance

matrix  $\mathbf{S}^H \mathbf{S} \in \mathbb{C}^{K \times K}$  in SCM  $\tilde{\mathbf{R}}$  [Eq. (2)]. Snapshot-data-based methods need more snapshots to obtain accurate estimates,<sup>6,20</sup> as confirmed for AP-Covariance and AP-Snapshot in Sec. VII.

## IV. ALTERNATING PROJECTIONS

AP-Covariance involves PSD projection [constraint in Eq. (10)] and  $K$ -rank Toeplitz projection [objective in Eq. (10)].

### A. PSD projection

The constraint Eq. (10) includes a Hermitian PSD matrix  $\mathbf{P}$ , which is obtained by projecting the constraint matrix onto the PSD set  $\mathcal{P}$ , defined by the PSD cone. The projection of  $\mathbf{P}$  onto the PSD set is achieved from the eigen-decomposition of  $\mathbf{P} \in \mathbb{C}^{2M \times 2M}$  with its eigenvalues  $\mu_i$  and eigenvectors  $\mathbf{q}_i$ ,  $\mathbf{P} = \sum_{i=1}^{2M} \mu_i \mathbf{q}_i \mathbf{q}_i^H$ ,<sup>28,29</sup>

$$P_{\mathcal{P}}(\mathbf{P}) = \sum_{i=1}^{2M} \max\{0, \mu_i\} \mathbf{q}_i \mathbf{q}_i^H. \quad (11)$$

### B. $K$ -rank Toeplitz projection

The objective [Eq. (10)] includes the SCM-related parameter  $\mathbf{R}$ , related to a  $K$ -rank Toeplitz matrix  $\mathbf{R}_o$ , i.e.,  $\mathbf{R} - \hat{\sigma}^2 \mathbf{I} = \mathbf{R}_o = \hat{\mathbf{A}} \text{diag}(\hat{\mathbf{p}}) \hat{\mathbf{A}}^H$ . The projection of  $\mathbf{R}$  onto the  $K$ -rank Toeplitz set  $\mathcal{R}$  is achieved as<sup>40,47</sup>

$$P_{\mathcal{R}}(\mathbf{R}) = \sum_{k=1}^K \hat{c}_k^2 \mathbf{a}(\hat{\theta}_k) \mathbf{a}^H(\hat{\theta}_k) = \hat{\mathbf{A}} \text{diag}(\hat{\mathbf{p}}) \hat{\mathbf{A}}^H, \quad (12)$$

$$\hat{\mathbf{p}} = \text{diag}\left(\hat{\mathbf{A}}^H \mathbf{R} (\hat{\mathbf{A}}^H)^H\right), \quad (13)$$

where  $\hat{\mathbf{A}} = [\mathbf{a}(\hat{\theta}_1) \dots \mathbf{a}(\hat{\theta}_K)] \in \mathbb{C}^{M \times K}$ ,  $\hat{\mathbf{A}}^H$  is the Moore-Penrose pseudo-inverse, and  $\text{diag}(\mathbf{A})$  is the column vector containing the diagonal elements of matrix  $\mathbf{A}$ . The factorization [Eq. (12)] represents the Vandermonde decomposition, which retrieves DOAs (Ref. 6, Sec. 11.6.2) DOAs  $\hat{\theta}_k$  [Eq. (12)] are obtained as in Sec. V. Once  $\hat{\theta}_k$  is recovered, the signal amplitudes are refined [Eq. (13)].<sup>2,47,48</sup> AP-Covariance iteratively updates  $\mathbf{R}$ , and the projection [Eq. (12)] keeps its signal part, i.e.,  $\mathbf{R}_{\text{old}} - \hat{\sigma}_{\text{old}}^2 \mathbf{I} = \mathbf{R}_{\text{new}}$ , resulting in a denoised SCM at convergence, i.e.,  $\mathbf{R}_{\text{new}} \rightarrow \mathbf{R}_o$ .

## V. ALGORITHMS FOR $K$ -RANK TOEPLITZ PROJECTION

Rank-constrained projection was achieved via eigendecomposition by computing the  $K$  largest eigenvalues.<sup>32,33,35,38</sup> The eigenvectors correspond to the signal subspace for DOA. We determine the signal components from the noise subspace and determine DOAs from the spectral peaks. It uses the concept that the signal is orthogonal to the noise and estimates the noise variance as the average of the smallest  $M-K$  eigenvalues of  $\mathbf{R}$ , similar to MUSIC.<sup>46</sup>

From root-MUSIC,<sup>45</sup> the common concepts are as follows:

- (1) Perform the eigendecomposition in signal and noise subspace, i.e.,  $\mathbf{R} = \mathbf{U}_S \Lambda_S \mathbf{U}_S^H + \mathbf{U}_N \Lambda_N \mathbf{U}_N^H$ .
- (2) Compute the null spectrum  $\mathcal{D}(z) = \mathbf{a}^H(z) \mathbf{U}_N \mathbf{U}_N^H \mathbf{a}(z)$ , where  $z = e^{-j(2\pi/\lambda)d \sin \theta}$  and  $\mathbf{a} = [z^{\delta_1} z^{\delta_2} \dots z^{\delta_M}]^T$ . {Recall the steering vector [Eq. (3)].}
- (3) Find the roots of  $\mathcal{D}(z)$  in complex  $z$ -plane by localizing the  $K$  lowest local minima of  $\mathcal{D}(z)$  on the unit circle  $|z| = 1$ ,

$$\hat{z} = \underset{|z|=1}{\operatorname{argmin}} \mathcal{D}(z), \quad k = 1, \dots, K, \quad (14)$$

$$\mathcal{D}(z_k) = \mathbf{a}^H(z_k) \mathbf{U}_N \mathbf{U}_N^H \mathbf{a}(z_k), \quad (15)$$

where  $\hat{z}_k = e^{-j(2\pi/\lambda)d \sin \hat{\theta}_k}$ .

- (4) DOAs are obtained,  $\hat{\theta}_k = -\sin^{-1}(\lambda \angle \hat{z}_k / 2\pi d)$ .
- (5) Refine the amplitudes of the corresponding  $\hat{\theta}_k$  from Eq. (13) and construct  $K$ -rank Toeplitz matrix using Eq. (12).

For finding roots of the null spectrum  $\mathcal{D}(z)$  [Eq. (14)], we propose algorithms for ULAs and NUAs.

### A. Algorithm for NUAs

Equation (14) is to find the roots of the null spectrum  $\mathcal{D}(z)$  [Eq. (15)]. For NUAs, an alternate expression to Eq. (15) is

$$\mathcal{D}(z) = \sum_{m=1}^M \sum_{n=1}^M w_{m,n} z^{-\delta_m + \delta_n}, \quad (16)$$

where  $w_{m,n}$  is element  $(m, n)$  of  $\mathbf{U}_N \mathbf{U}_N^H$ . To find roots of  $\mathcal{D}(z)$  in complex  $z$ -plane, we utilize the properties: the roots of interest lie on the unit circle (or appear in conjugate reciprocal pairs close to the unit circle); and for the phase angles of the corresponding roots,  $\mathcal{D}(z)$  on the unit circle has minima.<sup>23,40,45</sup> The optimization [Eq. (14)] with Eq. 16 is solved by a gridded search with an iterative grid refinement. An initial grid for  $z$  has 100  $M$  evenly spaced points in  $[-90^\circ, 90^\circ]$  on the unit circle  $|z| = 1$ , then the estimated minima locations are iteratively refined using golden section search. Reference 40 has extended root-MUSIC and AP-Snapshot to NUAs with accurate DOA performance for NUAs of arbitrary geometry. For the behavior of the null spectrum for NUAs, see Ref. 40, Sec. II.

### B. Algorithm for ULAs

For ULAs, we use a polynomial representation of  $\mathcal{D}(z)$  as  $\delta = [0 \ 1 \dots M-1]^T$  in Eq. (3). The steering vector is given as a polynomial vector,  $\mathbf{a} = [1 \ z^1 \dots z^{M-1}]^T$ , and Eq. (14) is to find the roots of the polynomials [Eq. (15)]. By replacing  $\delta_m = m-1$  and  $\delta_n = n-1$  in Eq. (16),  $\mathcal{D}(z)$  has a polynomial form as

$$\mathcal{D}(z) = \sum_{m=1}^M \sum_{n=1}^M w_{m,n} z^{-m+n}. \quad (17)$$

Finding roots [Eq. (14)] of polynomials [Eq. (17)] is solved efficiently, e.g., by converting it to the problem of finding

TABLE I. AP-Covariance algorithm: Input consists of SCM  $\tilde{\mathbf{R}}$ , the number of sources  $K$ , and the error threshold  $\epsilon_{\min}$ .

AP-Covariance for DOA estimation

1. Input:  $\tilde{\mathbf{R}} \in \mathbb{C}^{M \times M}$ ,  $K$ ,  $\epsilon_{\min} = 10^{-3}$
2. Initialization:  $\mathbf{R} \in \mathbb{C}^{M \times M}$ ,  $\mathbf{Z} \in \mathbb{C}^{M \times M}$  with uniformly  $(0, 1)$  distributed random for real and imaginary part.
3.  $\mathbf{R}^{\text{old}} = \mathbf{R}$ ,  $\mathbf{Z}^{\text{old}} = \mathbf{Z}$
4. while  $\|\mathbf{P} - \mathbf{P}^{\text{old}}\|_F < \epsilon_{\min}$  do
5.  $\mathbf{P} = \begin{bmatrix} \mathbf{R}^{\text{old}} & \tilde{\mathbf{R}} \\ \tilde{\mathbf{R}} & \mathbf{Z}^{\text{old}} \end{bmatrix}$
6. PSD projection:  $\mathbf{P} = P_{\mathcal{P}}(\mathbf{P})$  [Eq. (11)]
7.  $K$ -rank Toeplitz projection (Sec. V):  
 $\mathbf{R} = P_{\mathcal{R}}(\mathbf{R})$  [Eq. (12)]
8.  $\mathbf{P}(1 : M, 1 : M) = \mathbf{R}$
9.  $\mathbf{R}^{\text{old}} = \mathbf{R}$ ,  $\mathbf{Z}^{\text{old}} = \mathbf{P}(M + 1 : 2M, M + 1 : 2M)$
10. end while
11. Output:  $\mathbf{R}$

eigenvalues of the companion matrix of the polynomials. The procedure is the same as for root-MUSIC, except that DOAs  $\hat{\theta}_k$  are estimated from  $\mathbf{R}$  rather than SCM  $\tilde{\mathbf{R}}$ . For the behavior of the null spectrum for ULAs, see Ref. 40, Sec. II.

The procedure for AP-Covariance is summarized in Table I.

*Remark 1:* The earlier AP-Covariance<sup>41</sup> has separate projections,  $K$ -rank<sup>38</sup> and Toeplitz<sup>36</sup> projections. For Toeplitz matrix projection, the earlier version computes the average of the diagonal elements of  $\mathbf{R}$ <sup>36</sup> without information in  $\mathbf{R}$  after the PSD projection. The average-based Toeplitz projection makes matrix structure into Toeplitz matrix, but averaging the diagonal elements causes DOA biases. AP-Covariance reconstructs Toeplitz matrices preserving the obtained DOAs from the PSD projected  $\mathbf{R}$  (Sec. IVB) and propagates it to the following iterations, which gives a very good reconstruction (see Sec. VIA).

*Remark 2:* AP-Covariance can solve gridless DOA estimation for NUAs (see Fig. 1). Co-prime array is a special arbitrary NUAs as it is a sparse linear array by retaining only a part of a full ULA. The earlier AP-Covariance<sup>41</sup> solves the formulation choosing a subset of a full ULA. It estimates the full ULA SCM  $\mathbf{R}_{\text{full}}$  from its submatrix  $\Gamma \mathbf{R}_{\text{full}} \Gamma^T$  with an element-selection matrix  $\Gamma$ . The present algorithm deals with arbitrary configurations and achieves more accurate DOA estimates (see Fig. 6).

Earlier works used a pair of two arrays with multiplicative processing.<sup>49,50</sup> A disadvantage of this multiplicative processing is that for multiple coherent sources cross terms in the sample covariance matrix of the multiplicative array contain contributions that do not contain any physical contribution, e.g., Ref. 51, near Eq. (15). Alternative processing as in Refs. 52 and 53, sparse Bayesian processing,<sup>54–56</sup> or the AP processing used here do not suffer from cross terms.

*Remark 3:* The  $K$ -rank Toeplitz projection refines the DOA estimates using a subspace method. Subspace algorithms require a sufficient number of snapshots and are

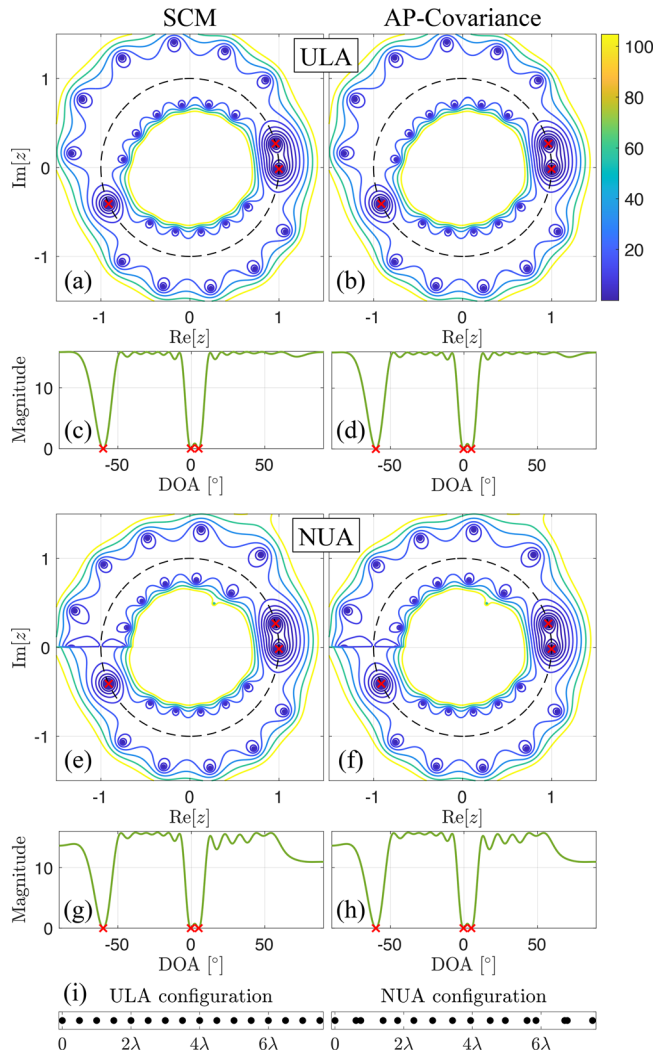


FIG. 1. (Color online) Null spectrum ( $|\mathcal{D}(z)|$ ) calculated with SCM (a) ULA, (e) NUA and evaluation on unit circle, (c) ULA, (g) NUA.  $|\mathcal{D}(z)|$  calculated with the estimated SCM parameter  $\mathbf{R}$  using (b) ULA [Eq. (17)], (f) NUA [Eq. (16)] and evaluation on unit circle, (d) ULA, (h) NUA for  $M = 16$ ,  $L = 16$ , and SNR 40 dB with DOAs  $[-60, -0.3, 5]^\circ$ , (i) The ULA and NUA structure.

infeasible with coherent sources due to a rank deficiency in SCM.

In contrast to subspace methods, the suggested method deals with single-snapshot data and coherent sources (see Sec. VIC). Conventional subspace methods determine the signal- and the noise-subspace by directly eigendecomposing the SCM. The suggested sparse method estimates the SCM-related matrix by exploiting DOAs in the SCM and decomposes it. Many sparse DOA estimation methods provide a high-resolution capability with single-snapshot data and with coherent sources.<sup>3,6,9,57–59</sup>

*Remark 4:* Equation (12) is a denoised SCM at convergence. The eigendecomposition of  $\mathbf{R}$  denoises the remaining eigenvectors, defined as a noise subspace that does not contain a signal component. There is still a noise component in the signal subspace, but the method provides very accurate DOA estimates. We have provided the estimation errors of

biased DOA estimates with the Cramér–Rao bound (CRB)<sup>60</sup> (see Sec. VII).

*Remark 5 (Local convergence):* AP-based algorithms are guaranteed to converge to the global optimum at a linear rate with all projections onto the convex sets.<sup>38,61</sup> However, as the rank-constrained projection is non-convex, the guarantees do not hold. As AP has good empirical performance, Refs. 32, 35, 38, and 61 have shown the local convergence of the rank-constrained projection and the effect of initialization has been investigated.<sup>33,34</sup> We use a random initialization as in Table I. A total of 1000 Monte Carlo simulations confirm that the success probability is close to 1 with fast convergence (see Sec. VII).

## VI. NULL SPECTRUM ANALYSIS

We study the null spectrum performance of the AP-based methods to indicate that AP-Covariance is preferable over AP-Snapshot.<sup>40</sup> A ULA and an NUA with  $M = 16$ ,  $L = 16$ , and a signal-to-noise ratio (SNR) 40 dB with DOAs  $[-60, -0.3, 5]^\circ$  are examined. The ULA has half-wavelength sensor spacing and the NUA is generated by adding random offsets from a uniform distribution between  $[-0.5, 0.5]^\circ$  (in half-wavelength units) to each sensor position except the first and the last sensors. The two arrays have the same array aperture.

The null spectrum is calculated by using Eq. (16) for NUAs and Eq. (17) for ULAs. Conventional subspace methods use the null spectrum, which is obtained by eigendecomposing the SCM  $\tilde{\mathbf{R}}$  [see Figs. 1(a), 1(c), 1(e), and 1(g)]. AP-Covariance uses the null spectrum obtained from the estimated  $\mathbf{R}$  [see Figs. 1(b), 1(d), 1(f), and 1(h)]. The null spectrum has minima on the unit circle at the true DOAs [see Figs. 1(c), 1(d), 1(g), and 1(h)], and solving Eq. (14) corresponds to the DOA estimation.

### A. Toeplitz projection

AP-Snapshot has two algorithms for NUA (Ref. 40, Algorithm 4) and ULA (Ref. 40, Algorithm 5). AP-Snapshot for ULAs and the earlier AP-Covariance have a separate projection, Toeplitz matrix projection [Ref. 40, Eq. (41) and Ref. 41, Eq. (17)]. It computes the average of the diagonal elements of  $\mathbf{R}$  without DOA information in  $\mathbf{R}$  after the PSD projection.

In Figs. 2(a)–2(d), same as in Fig. 1(d), we initialize the same  $\mathbf{R}$  and  $\mathbf{Z}$  ( $L = M$ ) for AP-Snapshot and AP-Covariance. The average-based Toeplitz projection makes matrix structure into Toeplitz matrix. However, it has worse projection performance with DOA biases [Fig. 2(b)], compared to AP-Covariance [Fig. 2(a)]. AP-Snapshot for NUAs without the average-based Toeplitz projection solves ULA cases and shows similar null spectrum performance to AP-Covariance. DOA estimation from the final  $\mathbf{R}$  results in  $0.0006^\circ$  error for AP-Covariance and  $0.3^\circ$  error for AP-Snapshot for ULAs [Figs. 2(c) and 2(d)], and  $0.002^\circ$  error for AP-Snapshot for NUAs. AP-Covariance reconstructs Toeplitz matrices preserving the obtained DOAs from the

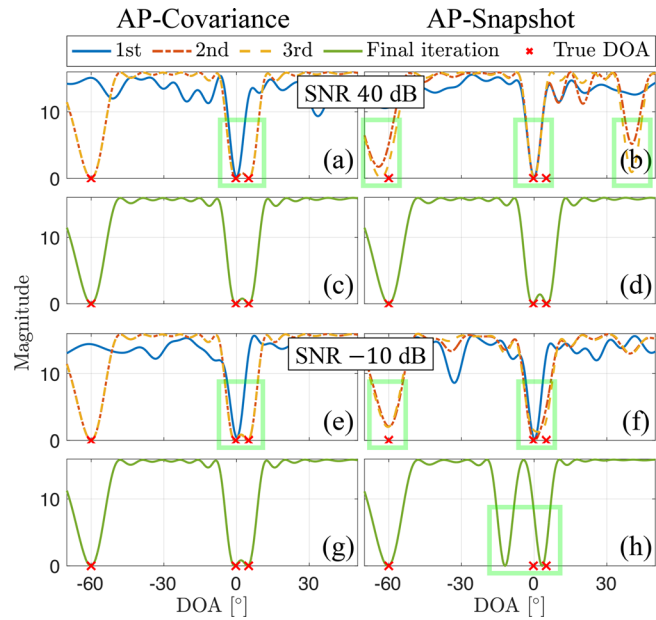


FIG. 2. (Color online) Null spectrum ( $|\mathcal{D}(z)|$ ) calculated with the estimated SCM parameter  $\mathbf{R}$  for (a), (c), (e), (g) AP-Covariance, (b), (d), (f), (h) AP-Snapshot. We extract  $\mathbf{R} (= P_{\mathcal{P}}(\mathbf{P}) (1 : M, 1 : M))$  after the PSD projection at each iteration. The ULA data is as in Figs. 1(a)–1(d). (a)–(d) with SNR 40 dB and  $-10$  dB, (e)–(h) RMSE, (c)  $0.0006^\circ$  for AP-Covariance, (d)  $0.3^\circ$  for AP-Snapshot, (g)  $0.41^\circ$ , (h)  $5.86^\circ$ .

PSD projected  $\mathbf{R}$  (Sec. IV B) and propagates it to the following iterations, which gives a very good reconstruction. We refer to AP-Snapshot for NUAs as AP-Snapshot hereafter.

### B. Covariance-fitting method

The covariance-fitting formulation in AP-Covariance projects DOAs in the data better than the snapshot-data-fitting. We initialize the same  $\mathbf{R}$  and  $\mathbf{Z}$  ( $L = M$ ) as Fig. 1(d) but with  $-10$  dB SNR, in Figs. 2(e)–2(h). We examine AP-Snapshot, AP-Covariance for ULAs (Sec. V B), and AP-Covariance for NUAs (Sec. V A). Two AP-Covariance for NUAs and ULAs show similar null spectrum performance and localize DOAs more accurately than AP-Snapshot. Note that AP-Covariance for NUAs and AP-Covariance for ULAs solve the same problem [Eq. (14)] but are based on Eqs. (16) and (17), respectively. AP-Snapshot for NUAs and AP-Covariance for NUAs use the same algorithm but are based on snapshot-data-fitting and covariance-fitting formulation, respectively. AP-Covariance projects DOAs well in the earlier iteration [Fig. 2(e)], compared to AP-Snapshot [Fig. 2(f)]. Similar performance is observed for single-snapshot and coherent source cases in Fig. 3. AP-Snapshot estimates one DOA in the middle of the two DOAs [Fig. 2(h)].

### C. Single snapshot and coherent sources

Many sparse methods for DOA utilize Toeplitz matrix reconstruction, and the Toeplitz representation is derived in the case of incoherent source signals and a large number of

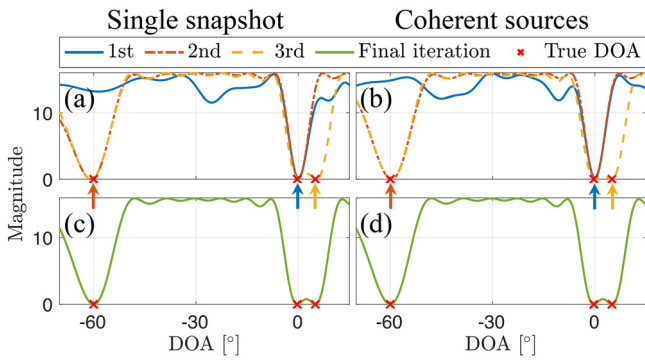


FIG. 3. (Color online) AP-Covariance performance as in Figs. 2(a) and 2(c). (a) and (c), with  $L = 1$  and (b) and (d), coherent sources RMSE: (c)  $0.008^\circ$ , (d)  $0.0006^\circ$ .

snapshots (Ref. 6, Sec. 11.6.2). (The source coherence is discussed in Sec. VII.) But this does not necessarily mean that they are applicable only for multiple snapshots with incoherent sources cases. The success of a Toeplitz approximation approach has been presented for single snapshot cases and coherent sources.<sup>8,21,26,40</sup>

We keep the scenario as in Fig. 2, but with a single snapshot case [Figs. 3(a) and 3(c)] and a coherent source case [Figs. 3(b) and 3(d)]. AP-Covariance shows better DOA projection over AP-Snapshot. For some cases, AP-Covariance projects one DOA at an iteration [Figs. 3(a) and 3(b)]. They exhibit slower convergence due to the Toeplitz approximation compared to the multiple snapshot incoherent source case [Fig. 2]. However, AP-Covariance outperforms AP-Snapshot. In many cases, AP-Snapshot merges the two closely located DOAs and provides poor performance as in Fig. 2(h) [see Figs. 4(a) and 4(c)]. The performance of DOA estimation with varying noise power and number of snapshots will be investigated in Sec. VII.

## VII. SIMULATION

The performance of AP-Covariance is compared with several DOA estimators: the earlier AP-Covariance (AP-Covariance ICASSP (the International Conference on Acoustics, Speech, and Signal Processing),<sup>41</sup> AP-Snapshot,<sup>40</sup> GLS with semi-definite programming solver (SDP-GLS),<sup>21</sup> sparse Bayesian learning (SBL),<sup>54,55,62</sup> MUSIC, and root-MUSIC,<sup>45</sup> as well as CRB.<sup>60</sup>

The SNR is defined,  $\text{SNR} = 10 \log_{10} [\mathbb{E}\{\|\mathbf{A}\mathbf{s}_l\|\}_2^2 / \mathbb{E}\{\|\mathbf{e}_l\|\}_2^2]$ , where  $\mathbf{s}_l \in \mathbb{C}^K$  and  $\mathbf{e}_l \in \mathbb{C}^M$ ,  $l = 1, \dots, L$ , are the source amplitude and the additive noise for the  $l$ th snapshot. The root mean squared error (RMSE) is,  $\text{RMSE} = \sqrt{\mathbb{E}[1/K \sum_{k=1}^K (\hat{\theta}_k - \theta_k)^2]}$ , where  $\hat{\theta}_k$  and  $\theta_k$  represent estimated and true DOA of the  $k$ th source. For DOA estimation methods having an angular search grid, the grid is discretized with  $[-90 : 1 : 90]^\circ$ . All results are based on 1000 Monte Carlo simulations.

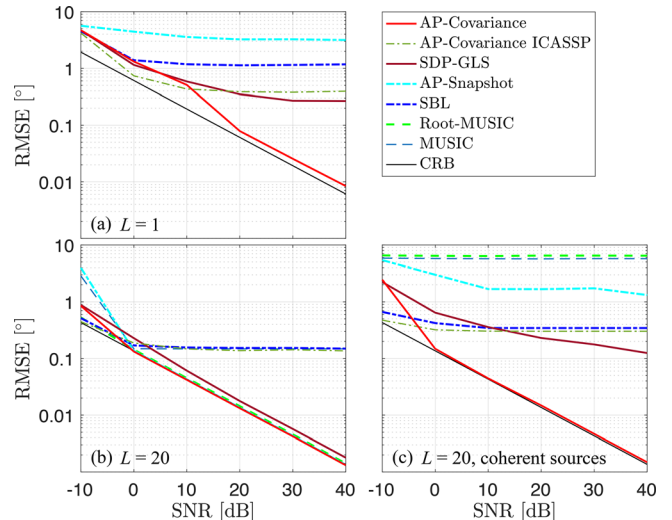


FIG. 4. (Color online) ULA SNR performance. The numbers of snapshots  $L$  are (a)  $L = 1$ , (b)  $L = 20$ , (c)  $L = 20$  but with coherent sources.

We examine an  $M = 16$  ULA with sensor spacing  $d = \lambda/2$ , i.e.,  $\boldsymbol{\delta} = [0 \ 1 \dots 15]^\top$  in Eq. (3). We consider four sources at DOAs  $[-60, -0.3, 5, 50]^\circ$  with equal magnitudes 20 dB or 10 (linear) with noise adjusted for each snapshot to have a specific SNR.

The DOA performance for ULAs is evaluated with the RMSE versus SNR (see Fig. 4). We consider scenarios with single snapshot, multiple snapshots, and coherent sources. SBL and MUSIC do not provide accurate DOAs even with high SNRs due to the grid mismatch for the DOA at  $0.3^\circ$ . MUSIC and root-MUSIC fail for coherent sources. AP-Covariance provides high-resolution and reliable DOA estimation even with a single snapshot and coherent sources, provides an improvement over SDP-GLS<sup>6,21</sup> and earlier AP-based methods,<sup>40,41</sup> and approaches the CRB at high SNRs.

Regarding the source coherence,<sup>63</sup> the source covariance matrix  $\mathbf{C}' \in \mathbb{C}^{K \times K}$  is calculated as

$$\mathbf{C}' = \mathbb{E}\left\{\mathbf{s}_l \mathbf{s}_l^\top\right\}, \quad l \in 1, \dots, L. \quad (18)$$

The coherence matrix for  $K$  sources  $\mathbf{C}$  is evaluated from  $\mathbf{C}'$ ,

$$C_{k',k''} = C'_{k',k''} / \sqrt{C'_{k',k'} C'_{k'',k''}}, \quad k', k'' \in 1, \dots, K. \quad (19)$$

The DOA performance is evaluated with the RMSE versus the number of snapshots  $L$  (see Fig. 5). We consider the same array as in Fig. 4 but with the number of sources,  $K = 2, 3$ , and  $4$ . AP-Covariance improves DOA performance significantly compared to AP-Covariance ICASSP and achieves robustness over AP-Snapshot with fewer snapshot data for  $K = 3$  and  $K = 4$  [see Figs. 5(b) and 5(c)].

We examine an  $M = 8$  co-prime array. A co-prime array involves two ULAs with spacing  $M_1 d$  and  $M_2 d$  where  $M_1$  and  $M_2$  are co-prime, i.e., their greatest common divisor

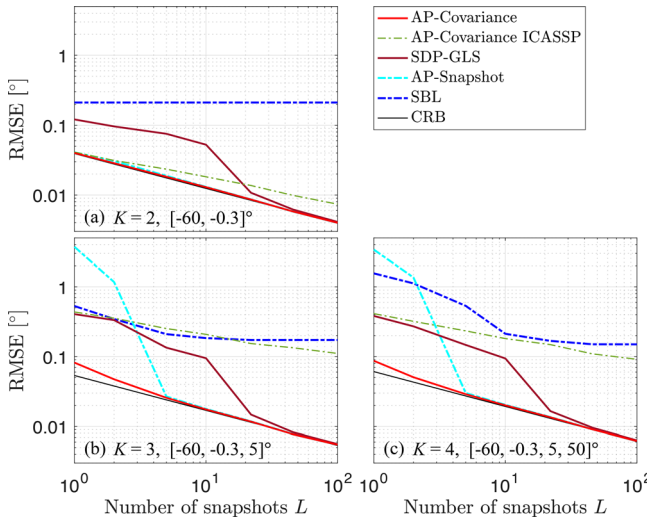


FIG. 5. (Color online) ULA Snapshot ( $L$ ) performance at SNR 20 dB. Incoherent sources are at DOAs (a)  $[-60, -0.3]^\circ$ , (b)  $[-60, -0.3, 5]^\circ$ , and (c)  $[-60, -0.3, 5, 50]^\circ$ .

is 1.<sup>42</sup> The two ULAs have  $\delta = [0 M_2 \cdots (M_1 - 1)M_2]^\top$  and  $\delta = [M_1 2M_1 \cdots (2M_2 - 1)M_1]^\top$ , a total of  $M_1 + 2M_2 - 1$  sensors. Here,  $M_1 = 5$  and  $M_2 = 2$  is used, i.e.,  $\delta = [0 2 4 5 6 8 10 15]^\top$  in Eq. (3).

The DOA performance with a co-prime array is evaluated with the RMSE versus SNR and  $L$  (see Fig. 6). MUSIC with co-array interpolation (MUSIC-I)<sup>64</sup> and Fourier domain root-MUSIC (FD root-MUSIC)<sup>23</sup> are also compared as DOA estimators for NUAs. AP-Covariance for NUAs offers similar performance with AP-Snapshot due to the performance of the  $K$ -rank Toeplitz projection algorithm for NUAs, but provides more accurate DOAs with fewer snapshot data as in Fig. 5(c).

AP-Covariance has additional computational merit over AP-Snapshot, when  $M \ll L$ , that AP-Covariance is a

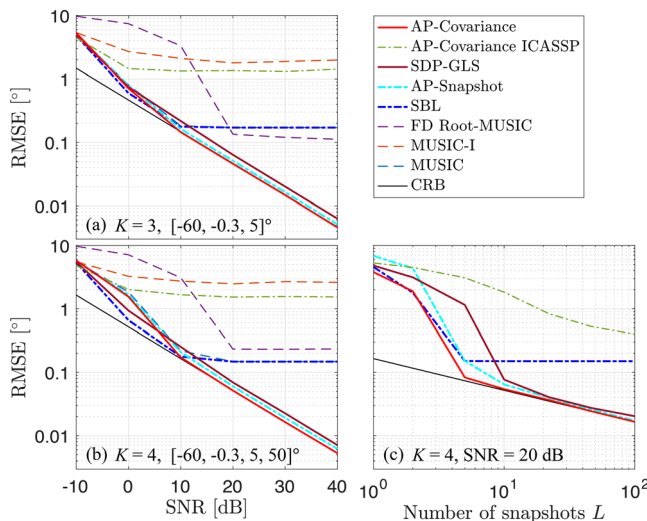


FIG. 6. (Color online) Co-prime array ( $M = 8$ ) performance. As in Fig. 4(b) but with  $L = 10$ ,  $K = 3$  sources at DOAs (a)  $[-60, -0.3, 5]^\circ$  and  $K = 4$  sources at DOAs, (b)  $[-60, -0.3, 5, 50]^\circ$ . As in Fig. 5(c) ( $K = 4$ ) at SNR 20 dB.

TABLE II. Average CPU time [s] (2.4 GHz Intel 8-core i9 processor). We consider  $K = 4$  at SNR 20 dB.

		AP-Covariance	AP-Snapshot	SDP-GLS	SBL
ULA	$M = 16, L = 20$	0.04	0.04	0.28	0.02
	$M = 16, L = 200$	0.04	0.16	0.28	0.02
	$M = 64, L = 20$	0.35	0.31	30.5	0.02
Co-prime	$M = 8, L = 20$	0.04	0.04	6.91	0.01
	$M = 8, L = 200$	0.04	0.18	7.84	0.01

covariance fitting algorithm and thus, the computational cost is independent of the number of snapshots (see Table II).

## VIII. EXPERIMENTAL RESULTS

We validate AP-Covariance using experimental data with a complex multipath shallow water environment. The dataset is from the SWellEx-96 experiment (shallow water evaluation cell experiment 1996),<sup>65–68</sup> conducted approximately 12 km from the tip of Point Loma near San Diego, CA. During the Event S5, from 23:15–00:30 GMT on 10–11 May, two sources, a shallow and a deep, were towed simultaneously from 8.65 km southwest to 2.90 km northeast of the vertical uniform linear array (VLA). The VLA has  $M = 64$  sensors with spacing  $d = 1.875$  m and was spanning 94.125–212.25 m depth. (Element 43 was corrupted and thus excluded.)

We focus on the deep source towed at 54 m depth at frequency 235 Hz. The data have a sampling frequency of 1500 Hz. The 1 min-duration data around 00:14 GMT is divided into 75% overlapping 100 snapshots. Each snapshot data is Fourier transformed with  $2^{12}$  samples. The duration data of 1 min covers 1 min after the point when the source was closest to the VLA.

To associate the estimated DOAs with multipath, we simulate the acoustic field using the Bellhop ray-tracing model.<sup>69</sup> We set environmental information as in Ref. 70. The characteristics of the underwater channel cause multipath. The source arrives at VLA with dominant strength via a direct path, a bottom-reflected, a surface-reflected, and a surface-bottom-reflected path (see Fig. 7).

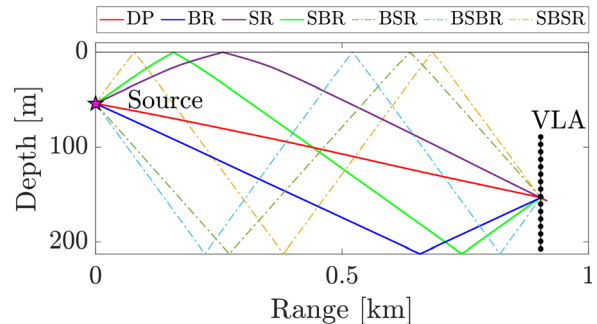


FIG. 7. (Color online) The SWellEx-96 experiment with multipath from the source and VLA in range and depth.

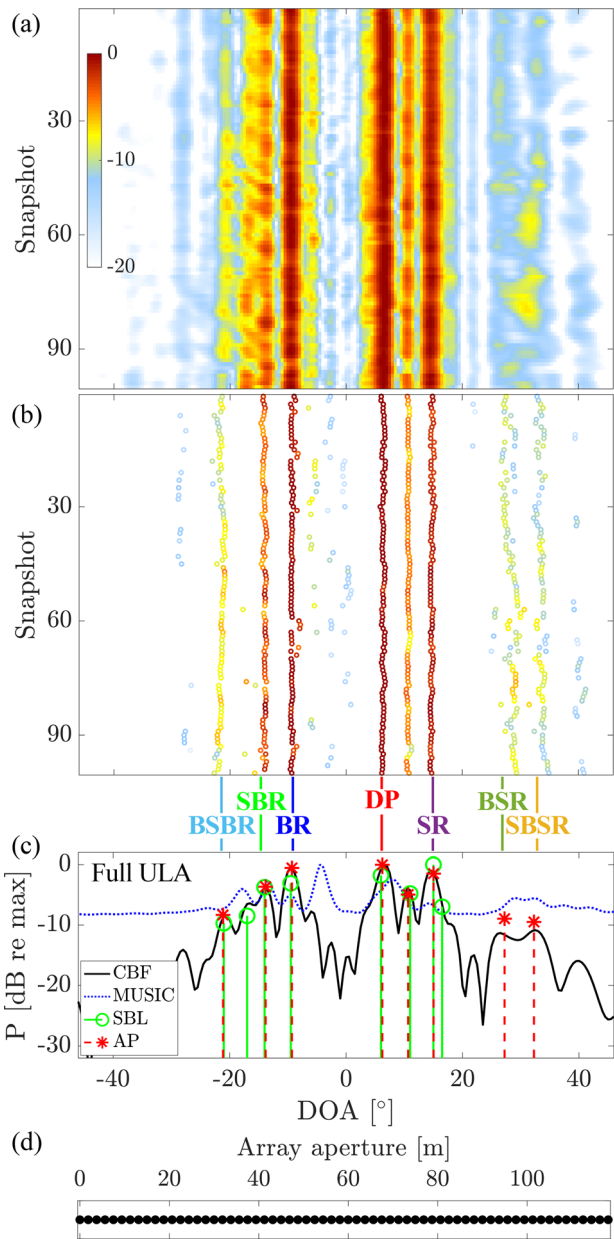


FIG. 8. (Color online) DOA estimation using acoustic data from the SWellEx-96 experiment. Single-snapshot processing for (a) CBF, (b) AP-Covariance. (c) Multiple snapshot processing for CBF, MUSIC, SBL, and AP-Covariance. (d) The full ULA structure. We have assumed  $K = 9$  sources for the single snapshot while for the multiple snapshot  $K = 8$ .

Single snapshot performance is presented [see Figs. 8(a) and 8(b)]. Sparse signal processing, SBL, and AP-Covariance, result in improved resolution relative to CBF. The estimated DOAs of SBL is similar to AP-Covariance, and the results are omitted. The DOAs for the simulated data in Fig. 7 are detected for the real data. DOA with dominant strength  $\sim 10^\circ$  corresponds to one possible path via a refracted path near the surface without reflections.

The processed data involve stationary DOAs over snapshots, which enables multiple snapshot processing to improve DOA performance. Figure 8(c) shows

multiple snapshot DOA performance, and the DOAs are coherent multipath arrivals. The coherent arrivals cause a rank deficiency in the SCM, and the MUSIC beamformer, a subspace method, fails. Sparse signal processing, SBL, and AP-Covariance, work well with single-snapshot data and multiple snapshot data with coherent arrivals.

Co-prime array performance is presented in Fig. 9. Based on the full ULA elements, see Fig. 8(d); various co-prime arrays are provided in Figs. 9(a)–9(e). Co-prime arrays avoid aliasing and provide resolution gain.<sup>54</sup> Sparse ULA [Fig. 9(f)] has intersensor spacing  $3d = 5.625 = 0.88\lambda$ , and all methods suffer from spatial aliasing. A co-prime array with the same array aperture with similar number of sensors [Fig. 9(a)] significantly mitigates spatial aliasing.

Co-prime array performance becomes poor as  $M_2$  gets higher and the array has coarse element spacing. The co-prime array with  $M_1 = 13, M_2 = 2$  [Fig. 9(b)] outperforms over the co-prime array with  $M_1 = 11, M_2 = 3$  [Fig. 9(c)], although both have the same number of elements and the latter has larger array aperture. Within full ULA 64 elements, we can configure different cases with the same array geometry by shifting the element number, e.g., the same structure as Fig. 9(b) but start from the array element 2. We found more successful cases with the co-prime in Fig. 9(b) than Fig. 9(e). A co-prime array with  $M_1 = 6, M_2 = 5$  ( $M = 15$ ) has 101.25 m array aperture, larger than Figs. 9(b), 9(d), and 9(e), but fails and is thus excluded. Using co-prime arrays, we can save the sensors by about a quarter. AP-Covariance and SBL can accurately identify DOAs using co-prime arrays.

## IX. CONCLUSION

We introduced a gridless sparse direction-of-arrival (DOA) estimation method. The existing gridless sparse methods require solving semidefinite programming in its formulation, which is computationally expensive. The suggested method uses Toeplitz-structured low-rank matrix reconstruction, which alternating projections efficiently solve. The DOA error analysis showed that the method outperforms state-of-the-art methods in accuracy and speed. The method uses covariance fitting, which additionally reduces the computational cost for a large number of snapshot data.

The proposed method deals with non-uniform linear arrays, including co-prime. Using co-prime arrays with the method accurately estimates DOAs with fewer elements than full uniform linear arrays and avoids spatial aliasing.

Numerical evaluation indicated the algorithm is competitive to other methods and approaches to the Cramér–Rao bound at high SNR. The method performs well for single-snapshot data and multiple snapshot data with coherent sources. Good performance was demonstrated on real data, including co-prime array performance.

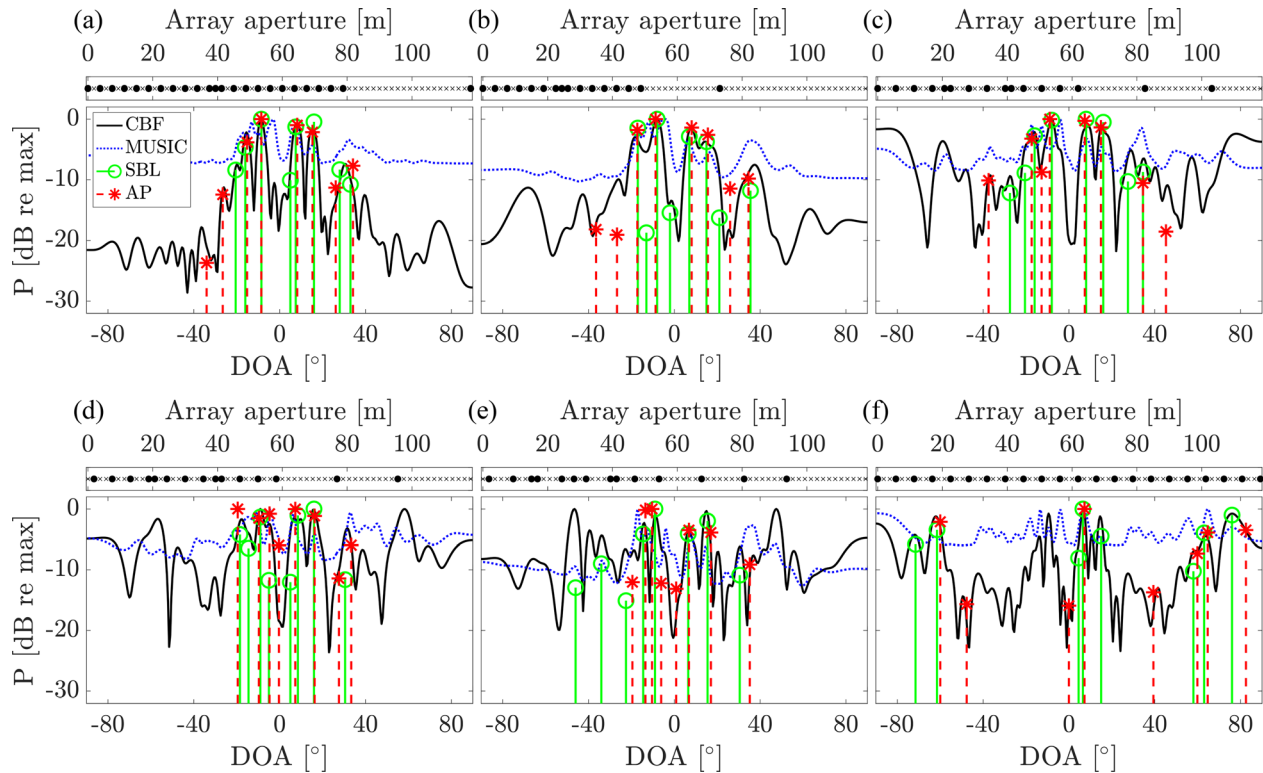


FIG. 9. (Color online) As in Fig. 8(c) but with sparse array geometries: (a)–(e) co-prime arrays, (f) ULA with  $3d$  ( $M = 22$ ). Co-prime arrays consist of two ULAs with spacing  $M_1 d$  and  $M_2 d$  such that  $M_1$  and  $M_2$  are co-prime: (a)  $M_1 = 21$ ,  $M_2 = 2$  ( $M = 24$ ), (b)  $M_1 = 13$ ,  $M_2 = 2$  ( $M = 16$ ), (c)  $M_1 = 11$ ,  $M_2 = 3$  ( $M = 16$ ), (d)  $M_1 = 10$ ,  $M_2 = 3$  ( $M = 15$ ), (e)  $M_1 = 7$ ,  $M_2 = 4$  ( $M = 14$ ).

## ACKNOWLEDGMENTS

This research was supported by the Office of Naval Research, Grant No. N00014-21-1-2267.

- <sup>1</sup>D. Malioutov, M. Cetin, and A. S. Willsky, “A sparse signal reconstruction perspective for source localization with sensor arrays,” *IEEE Trans. Signal Process.* **53**(8), 3010–3022 (2005).
- <sup>2</sup>A. Xenaki, P. Gerstoft, and K. Mosegaard, “Compressive beamforming,” *J. Acoust. Soc. Am.* **136**(1), 260–271 (2014).
- <sup>3</sup>P. Gerstoft, A. Xenaki, and C. F. Mecklenbräuker, “Multiple and single snapshot compressive beamforming,” *J. Acoust. Soc. Am.* **138**(4), 2003–2014 (2015).
- <sup>4</sup>A. Xenaki and P. Gerstoft, “Grid-free compressive beamforming,” *J. Acoust. Soc. Am.* **137**(4), 1923–1935 (2015).
- <sup>5</sup>Y. Park, Y. Choo, and W. Seong, “Multiple snapshot grid free compressive beamforming,” *J. Acoust. Soc. Am.* **143**(6), 3849–3859 (2018).
- <sup>6</sup>Z. Yang, J. Li, P. Stoica, and L. Xie, “Sparse methods for direction-of-arrival estimation,” in *Academic Press Library in Signal Processing: Array, Radar and Communications Engineering* (Academic Press, Cambridge, MA, 2018), Vol. 7, Chap. 11, pp. 509–581.
- <sup>7</sup>P. Gerstoft, C. F. Mecklenbräuker, W. Seong, and M. Bianco, “Introduction to compressive sensing in acoustics,” *J. Acoust. Soc. Am.* **143**(6), 3731–3736 (2018).
- <sup>8</sup>P. Stoica, P. Babu, and J. Li, “SPICE: A sparse covariance-based estimation method for array processing,” *IEEE Trans. Signal Process.* **59**(2), 629–638 (2011).
- <sup>9</sup>R. R. Pote and B. D. Rao, “Robustness of sparse Bayesian learning in correlated environments,” in *Proc. IEEE International Conference on Acoustics, Speech, and Signal Processing (ICASSP)*, May 4–8, Barcelona, Spain (2020), pp. 9100–9104.
- <sup>10</sup>E. Candès and C. Fernandez-Granda, “Towards a mathematical theory of super-resolution,” *Commun. Pure Appl. Math.* **67**(6), 906–956 (2014).
- <sup>11</sup>G. Tang, B. N. Bhaskar, P. Shah, and B. Recht, “Compressed sensing off the grid,” *IEEE Trans. Inf. Theory* **59**(11), 7465–7490 (2013).
- <sup>12</sup>Y. Chi, L. L. Scharf, A. Pezeshki, and A. R. Calderbank, “Sensitivity to basis mismatch in compressed sensing,” *IEEE Trans. Signal Process.* **59**(5), 2182–2195 (2011).
- <sup>13</sup>P. Pal and P. P. Vaidyanathan, “A grid-less approach to underdetermined direction of arrival estimation via low rank matrix denoising,” *IEEE Signal Process. Lett.* **21**(6), 737–741 (2014).
- <sup>14</sup>Y. Chi and M. F. D. Costa, “Harnessing sparsity over the continuum: Atomic norm minimization for superresolution,” *IEEE Signal Process. Mag.* **37**(2), 39–57 (2020).
- <sup>15</sup>Y. Wang, Y. Zhang, Z. Tian, G. Leus, and G. Zhang, “Super-resolution channel estimation for arbitrary arrays in hybrid millimeter-wave massive MIMO systems,” *IEEE J. Sel. Top. Signal Process.* **13**(5), 947–960 (2019).
- <sup>16</sup>A. G. Raj and J. H. McClellan, “Super-resolution DOA estimation for arbitrary array geometries using a single noisy snapshot,” in *Proc. IEEE International Conference on Acoustics, Speech, and Signal Processing*, May 12–17, Brighton, UK (2019), pp. 4145–4149.
- <sup>17</sup>S. Semper, F. Roemer, T. Hotz, and G. D. Gallo, “Grid-free direction-of-arrival estimation with compressed sensing and arbitrary antenna arrays,” in *Proc. IEEE International Conference on Acoustics, Speech, and Signal Processing (ICASSP)*, April 15–20, Calgary, Canada (2018), pp. 3251–3255.
- <sup>18</sup>Y. Yang, Z. Chu, Z. Xu, and G. Ping, “Two-dimensional grid-free compressive beamforming,” *J. Acoust. Soc. Am.* **142**(2), 618–629 (2017).
- <sup>19</sup>G. Chardon and U. Boureau, “Gridless three-dimensional compressive beamforming with the Sliding Frank-Wolfe algorithm,” *J. Acoust. Soc. Am.* **150**(4), 3139–3148 (2021).
- <sup>20</sup>C. Steffens, M. Pesavento, and M. E. Pfetsch, “A compact formulation for the  $\ell_{2,1}$  mixed-norm minimization problem,” *IEEE Trans. Signal Process.* **66**(6), 1483–1497 (2018).
- <sup>21</sup>Z. Yang and L. Xie, “On gridless sparse methods for line spectral estimation from complete and incomplete data,” *IEEE Trans. Signal Process.* **63**(12), 3139–3153 (2015).
- <sup>22</sup>M. Sánchez-Fernández, V. Jamali, J. Llorca, and A. M. Tulino, “Gridless multidimensional angle-of-arrival estimation for arbitrary 3D antenna arrays,” *IEEE Trans. Wireless Commun.* **20**(7), 4748–4764 (2021).

- <sup>23</sup>M. Rubsamen and A. B. Gershman, "Direction-of-arrival estimation for nonuniform sensor arrays: From manifold separation to Fourier domain MUSIC methods," *IEEE Trans. Signal Process.* **57**(2), 588–599 (2009).
- <sup>24</sup>X. Wu, W. Zhu, and J. Yan, "A Toeplitz covariance matrix reconstruction approach for direction-of-arrival estimation," *IEEE Trans. Veh. Technol.* **66**(9), 8223–8237 (2017).
- <sup>25</sup>M. Trinh-Hoang, M. Viberg, and M. Pesavento, "Partial relaxation approach: An eigenvalue-based DOA estimator framework," *IEEE Trans. Signal Process.* **66**(23), 6190–6203 (2018).
- <sup>26</sup>S. Y. Kung, C. Lo, and R. Foka, "A Toeplitz approximation approach to coherent source direction finding," in *Proc. IEEE International Conference on Acoustics, Speech, and Signal Processing (ICASSP)*, April 7–11, Tokyo, Japan (1986), pp. 193–196.
- <sup>27</sup>S. Liu, Z. Mao, Y. D. Zhang, and Y. Huang, "Rank minimization-based Toeplitz reconstruction for DOA estimation using coprime array," *IEEE Commun. Lett.* **25**(7), 2265–2269 (2021).
- <sup>28</sup>S. Boyd and L. Vandenberghe, *Convex Optimization* (Cambridge University Press, Cambridge, UK, 2004).
- <sup>29</sup>J. Dattorro, *Convex Optimization & Euclidean Distance Geometry* (Meboo Publishing USA, Palo Alto, CA, 2010).
- <sup>30</sup>H. Q. Cai, J.-F. Cai, and K. Wei, "Accelerated alternating projections for robust principal component analysis," *J. Mach. Learn. Res.* **20**(1), 685–717 (2019).
- <sup>31</sup>X. Jiang, Z. Zhong, X. Liu, and H. C. So, "Robust matrix completion via alternating projection," *IEEE Signal Process. Lett.* **24**(5), 579–583 (2017).
- <sup>32</sup>H. Q. Cai, J.-F. Cai, T. Wang, and G. Yin, "Accelerated structured alternating projections for robust spectrally sparse signal recovery," *IEEE Trans. Signal Process.* **69**(18), 809–821 (2021).
- <sup>33</sup>I. Waldspurger, "Phase retrieval with random Gaussian sensing vectors by alternating projections," *IEEE Trans. Inf. Theory* **64**(5), 3301–3312 (2018).
- <sup>34</sup>P. Chen, A. Fannjiang, and G.-R. Liu, "Phase retrieval with one or two diffraction patterns by alternating projections with the null initialization," *J. Fourier Anal. Appl.* **24**(3), 719–758 (2018).
- <sup>35</sup>P. Netrapalli, P. Jain, and S. Sanghavi, "Phase retrieval using alternating minimization," *IEEE Trans. Signal Process.* **63**(18), 4814–4826 (2015).
- <sup>36</sup>M. Cho, J. Cai, S. Liu, Y. C. Eldar, and W. Xu, "Fast alternating projected gradient descent algorithms for recovering spectrally sparse signals," in *Proc. IEEE International Conference on Acoustics, Speech, and Signal Processing* (2016), pp. 4638–4642.
- <sup>37</sup>L. Condat and A. Hirabayashi, "Cazdow denoising upgraded: A new projection method for the recovery of Dirac pulses from noisy linear measurements," *Sampl. Theory Signal Image Process.* **14**(1), 17–47 (2015).
- <sup>38</sup>P. Jain, R. Meka, and I. Dhillon, "Guaranteed rank minimization via singular value projection," in *International Conference on Neural Information Processing Systems (NIPS 2010)*, December 6–9, Vancouver, Canada (2010), Vol. 23.
- <sup>39</sup>M. Wagner, P. Gerstoft, and Y. Park, "Gridless DOA estimation via alternating projections," in *Proc. IEEE International Conference on Acoustics, Speech, and Signal Processing* (2010), pp. 4215–4219.
- <sup>40</sup>M. Wagner, Y. Park, and P. Gerstoft, "Gridless DOA estimation and root-MUSIC for non-uniform linear arrays," *IEEE Trans. Signal Process.* **69**, 2144–2157 (2021).
- <sup>41</sup>Y. Park and P. Gerstoft, "Alternating projections gridless covariance-based estimation for DOA," in *Proc. IEEE International Conference on Acoustics, Speech, and Signal Processing*, June 6–11, Barcelona, Spain (2021), pp. 4385–4389.
- <sup>42</sup>P. P. Vaidyanathan and P. Pal, "Sparse sensing with co-prime samplers and arrays," *IEEE Trans. Signal Process.* **59**(2), 573–586 (2011).
- <sup>43</sup>P. Gerstoft, R. Menon, W. S. Hodgkiss, and C. F. Mecklenbräuker, "Eigenvalues of the sample covariance matrix for a towed array," *J. Acoust. Soc. Am.* **132**(4), 2388–2396 (2012).
- <sup>44</sup>P. Gerstoft, C. F. Mecklenbräuker, A. Xenaki, and S. Nannuru, "Multisnapshot sparse Bayesian learning for DOA," *IEEE Signal Process. Lett.* **23**(10), 1469–1473 (2016).
- <sup>45</sup>B. D. Rao and K. V. S. Hari, "Performance analysis of root-MUSIC," *IEEE Trans. Acoust. Speech, Signal Process.* **37**(12), 1939–1949 (1989).
- <sup>46</sup>H. Qiao and P. Pal, "Guaranteed localization of more sources than sensors with finite snapshots in multiple measurement vector models using difference co-arrays," *IEEE Trans. Signal Process.* **67**(22), 5715–5729 (2019).
- <sup>47</sup>S. J. Wright, R. D. Nowak, and M. A. T. Figueiredo, "Sparse reconstruction by separable approximation," *IEEE Trans. Signal Process.* **57**(7), 2479–2493 (2009).
- <sup>48</sup>E. Candès and C. Fernandez-Granda, "Super-resolution from noisy data," *J. Fourier Anal. Appl.* **19**(6), 1229–1254 (2013).
- <sup>49</sup>K. Adhikari and J. R. Buck, "Spatial spectral estimation with product processing of a pair of colinear arrays," *IEEE Trans. Signal Process.* **65**(9), 2389–2401 (2017).
- <sup>50</sup>K. Wage, "When two wrongs make a right: Combining aliased arrays to find sound sources," *Acoust. Today* **14**(3), 48–56 (2018).
- <sup>51</sup>Y. Hu, Y. Liu, and X. Wang, "DOA estimation of coherent signals on coprime arrays exploiting fourth-order cumulants," *Sensors* **17**(4), 682 (2017).
- <sup>52</sup>G. Di Martino and A. Iodice, "Coprime synthetic aperture radar (CopSAR): A new acquisition mode for maritime surveillance," *IEEE Trans. Geosci. Remote Sens.* **53**(6), 3110–3123 (2015).
- <sup>53</sup>Y. Liu and J. R. Buck, "Gaussian source detection and spatial spectral estimation using a coprime sensor array with the min processor," *IEEE Trans. Signal Process.* **66**(1), 186–199 (2018).
- <sup>54</sup>S. Nannuru, A. Koochakzadeh, K. L. Gemba, P. Pal, and P. Gerstoft, "Sparse Bayesian learning for beamforming using sparse linear arrays," *J. Acoust. Soc. Am.* **144**(5), 2719–2729 (2018).
- <sup>55</sup>S. Nannuru, P. Gerstoft, A. Koochakzadeh, and P. Pal, "Sparse Bayesian learning for DOA estimation using co-prime and nested arrays," in *Proc. 10th IEEE Sensor Array and Multichannel Signal Processing Workshop (SAM)*, July 8–11, Sheffield, UK (2018), pp. 519–523.
- <sup>56</sup>J. Dai and H. C. So, "Real-valued sparse Bayesian learning for DOA estimation with arbitrary linear arrays," *IEEE Trans. Signal Process.* **69**, 4977–4990 (2021).
- <sup>57</sup>Y. Zhang, Y. Yang, L. Yang, and Y. Wang, "Off-grid DOA estimation of correlated sources for nonuniform linear array through hierarchical sparse recovery in a Bayesian framework and asymptotic minimum variance criterion," *Signal Process.* **178**, 107813 (2021).
- <sup>58</sup>Y. Ma, X. Cao, X. Wang, M. S. Greco, and F. Gini, "Multi-source off-grid DOA estimation with single snapshot using non-uniform linear arrays," *Signal Process.* **189**, 108238 (2021).
- <sup>59</sup>A. Das, W. S. Hodgkiss, and P. Gerstoft, "Coherent multipath direction-of-arrival resolution using compressed sensing," *IEEE J. Ocean. Eng.* **42**(2), 494–505 (2017).
- <sup>60</sup>P. Stoica and A. Nehorai, "MUSIC, maximum likelihood, and Cramér-Rao bound," *IEEE Trans. Acoust., Speech, Signal Process.* **37**(5), 720–741 (1989).
- <sup>61</sup>A. S. Lewis, D. R. Luke, and J. Malick, "Local linear convergence for alternating and averaged nonconvex projections," *Found. Comput. Math.* **9**, 485–513 (2009).
- <sup>62</sup>S. Nannuru, K. L. Gemba, and P. Gerstoft, "SBL4: Matlab software for sparse Bayesian learning, version 4" (2016) <http://github.com/gerstoft/SBL> (Last viewed April 21, 2022).
- <sup>63</sup>C. F. Mecklenbräuker, P. Gerstoft, and G. Leus, "Sparse Bayesian learning for DOA estimation of correlated sources," in *Proc. 10th IEEE Sensor Array and Multichannel Signal Processing Workshop (SAM)*, July 8–11, Sheffield, UK (2018), pp. 533–537.
- <sup>64</sup>C. Liu and P. P. Vaidyanathan, "Remarks on the spatial smoothing step in coarray MUSIC," *IEEE Signal Process. Lett.* **22**(9), 1438–1442 (2015).
- <sup>65</sup>N. O. Booth, P. A. Baxley, J. A. Rice, P. W. Schey, W. S. Hodgkiss, G. L. D'Spain, and J. J. Murray, "Source localization with broad-band matched-field processing in shallow water," *IEEE J. Ocean. Eng.* **21**(4), 402–412 (1996).
- <sup>66</sup>K. L. Gemba, S. Nannuru, and P. Gerstoft, "Robust ocean acoustic localization with sparse Bayesian learning," *IEEE J. Sel. Top. Signal Process.* **13**(1), 49–60 (2019).
- <sup>67</sup>Y. Park, F. Meyer, and P. Gerstoft, "Sequential sparse Bayesian learning for time-varying direction of arrival," *J. Acoust. Soc. Am.* **149**(3), 2089–2099 (2021).
- <sup>68</sup>F. Meyer and K. L. Gemba, "Probabilistic focalization for shallow water localization," *J. Acoust. Soc. Am.* **150**(2), 1057–1066 (2021).
- <sup>69</sup>M. B. Porter, "Acoustic toolbox," <http://oalib.hlsresearch.com/AcousticsToolbox> (Last viewed April 21, 2022).
- <sup>70</sup>G. L. D'Spain, J. J. Murray, W. S. Hodgkiss, N. O. Booth, and P. W. Schey, "Mirages in shallow water matched field processing," *J. Acoust. Soc. Am.* **105**(6), 3245–3265 (1999).